A Critical Evaluation of Direct Energy Transfer as a Tool for Analysis of Nanoscale Morphologies in Polymers. Application to Block Copolymer Interfaces

Ahmad Yekta,[†] **John G. Spiro,**[‡] **and Mitchell A. Winnik***

Department of Chemistry, University of Toronto, 80 St. George St., Toronto, Ontario, Canada M5S 3H6

Received: April 29, 1998; In Final Form: July 9, 1998

Simulations of energy-transfer kinetics were carried out for a lamellar block copolymer system in which donor and acceptor dyes were attached to the block junction. In such a system, the distribution of donors and acceptors follows $P_J(z)$, which describes the distribution of the junctions across the interface. We use these simulations to examine the type of information about the block copolymer morphology available from analysis of fluorescence decay profiles generated by these systems. Within the context of a Helfand−Tagami distribution for $P_J(z)$, one can obtain reliable estimates of the ratio of the period spacing to interface thickness (H/δ) but not the individual parameters H and δ. Since H can be determined independently in a scattering experiment, this approach is useful for obtaining values of δ with better than 5% accuracy. Attempts to distinguish a Helfand−Tagami profile from a Gaussian profile were not successful. The energy-transfer experiment may be employed to reject the wrong morphology only if prior values of H and δ are determined by other methods.

Introduction

The characteristic feature of most polymer mixtures is that the components do not mix on a macroscopic scale. Binary blends of most homopolymers not only form separate phases but the sizes of the domains often depend on the processing history of the sample.[1] If one or both of the components are rigid glasses at room temperature, then the morphology generated during processing is frozen in the material. Diblock copolymers represent a special case of a system composed of two polymer components attached at a common junction. If the polymer molecules are similar in length and composition and the two components have limited miscibility, then the components will form separate phases. The degree of phase separation is limited by the covalent bond between the two polymers, and in order to satisfy the space-filling requirements of uniform density, such systems self-assemble into periodic structures. If the two polymers are approximately the same length, a periodic lamellar structure is formed.[2−4]

One of the most interesting topics in contemporary polymer science involves the characterization of the interface between polymer domains. These interfaces are important because the macroscopic mechanical properties of the material depend on adhesion and the transfer of stresses across the interface, as, for example, in impact modified plastics. Unlike inorganic materials, where interfaces are sharp and characterized by thicknesses of at most a few angstroms, polymer−polymer interfaces are by comparison more diffuse. In the few instances where reliable data are available, values ranging from 2 to 8 nm are found. The theoretical description of polymer interfaces begins with consideration of the Flory χ parameter, which describes the free energy of interaction between the repeating units of the two polymers. While χ has a value larger than zero in immiscible blends, the values are often small. In these situations, a significant extent of segment interpenetration occurs between the two components at the domain interface. The theory of block copolymer interfaces reveals that block copolymer interfaces and polymer blend interfaces share many common features. The major difference in the free energy of interface formation is the entropy penalty for localization of the joints in the interface for block copolymers. This term becomes smaller as the polymers become longer, and for long chains, the interface thicknesses are predicted to be the same in both systems.

Over the past decade, there have been major advances in our ability to study polymer interfaces. The most powerful technique is neutron reflectivity (NR), in which one observes the specular reflection between thin films of the two polymers and contrast is obtained by selective deuteration of one of the components.[4−7] This technique is equally powerful for the study of both blends and self-assembling block copolymers but is limited to the lamellar geometry. Small-angle neutron scattering (SANS) and small-angle X-ray scattering (SAXS) experiments are both sensitive to the sharpness or diffuseness of the interface between components of different contrast factors, but the interpretation of the data is not as rigorous as in the case of NR. Here, one looks for deviations from Porod−Law scattering in a region where the scattering intensity is weak. Both NR and scattering techniques are sensitive to other factors such as waviness at the interface, which increase the apparent diffuseness of the interface, and the data require appropriate corrections.[8]

Alternative approaches to study polymer interfaces would be very useful. One possibility involves nonradiative energy-transfer (ET) experiments between fluorescent dyes attached at low levels of labeling to the two components. The number of groups actively employing this technique has been small. Fredrickson was first to point out the utility of this type of experiment for junction-labeled block copolymers.[9] Actual

* To whom correspondence may be addressed. E-mail: mwinnik@chem.utoronto.ca.
† Current address: Imaging Research Inc., 500 Glenridge Ave., Brock University, St. Catharines, Ontario, Canada L2S 3A1. Telephone: (905)-688-2040. Fax: (905)685-5861. E-mail: Imaging@spartan.ac.brocku.ca.
‡ E-mail: jspiro@chem.utoronto.ca.

Analysis of Nanoscale Morphologies in Polymers

J. Phys. Chem. B, Vol. 102, No. 41, 1998 **7961**

experimentation with specifically labeled block copolymers required waiting until particular synthetic difficulties were overcome.[10,11] More recently, Farinha et al.[12] used simulations to show that such experiments cannot distinguish between planar and spherical interfaces if the radius of the spherical domain is greater than the critical Förster radius R_o. The rate of ET is very sensitive to the donor−acceptor (D/A) separation distance r, and a diffuse interface brings more D and A groups into proximity. Phase separation leads to confinement of the dyes in the interface. The kinetics and quantum efficiency of ET will be very sensitive to the donor−acceptor distance distribution, which in turn depends on the distribution of the junction points in the interface.

For these tools to be employed properly, we need an appropriate theory of energy transfer in the restricted dimensions of the interface. This theory needs to be tested through simulations that examine the extent to which data obtained through experiment will be sensitive to the morphological features of the interface. Finally, model data and experimental data need to be compared to see if real systems involve features of the morphology neglected in the simulations.

Here, we present our first steps toward achieving this goal. The particular system we choose to examine is the interfacial domains of lamellar structures formed by block copolymer melts. In this paper, we address two specific questions. (1) Can an ET experiment determine the shape (morphology) of a polymer−polymer interface, i.e., the shape of the distribution of segments or junctions across the interface? For example, mean-field theory predicts a Helfand−Tagami (HT) distribution for the junctions across a block copolymer interface and a Gaussian distribution of chain ends across the center of a lamellar domain.[13,14] While both distributions are "bell-shaped", the Gaussian distribution is more peaked with a smaller fraction of the distribution in the tails. Can we distinguish a Gaussian from an HT distribution in an ET experiment? (2) Assuming a given morphology, what are the analytical limits in quantitative recovery of the system parameters. The two parameters that characterize the local morphology of a lamellar block copolymer system are the period spacing H and the interface thickness δ. Assuming, for example, an HT distribution of junctions, can one recover both H and δ in a single ET experiment or in a series of ET experiments?

To proceed, we first give a brief review of the theory of energy transfer and then examine the specific features of the theory that have to be taken into account in applications to diffuse interfaces, which are characterized by a distribution of both donor and acceptor groups. We then describe the simulation of ET experiments using examples that approximate two systems previously examined, poly(styrene-*b*-methyl methacrylate) [PS−PMMA] block copolymers[10] and poly(isoprene-*b*-methyl methacrylate) [PI−PMMA] block copolymers.[11] Our major conclusions in the context of these simulations will be, first, that one cannot without other information distinguish HT from Gaussian distribution profiles. Second, assuming a theoretical distribution profile, one can with good confidence determine H/δ values. While in principle one can separate the data to obtain the independent parameters, the χ-squared surface is rather flat. A much more sensible strategy would be to determine H from a scattering experiment and combine it with H/δ values determined in an ET experiment.

Energy Transfer and Morphology

Since the pioneering work of Förster,[15] many studies, both theoretical and experimental, have established that if certain experimental conditions are met, an electronically excited fluorescent molecule (donor D*) may transfer its energy to another, nearby ground-state molecule (acceptor A), forming D and A* as byproducts.[16] The rate of energy transfer $w(r)$ depends on the D−A separation distance r, and is given by the expression

$$w(r) = \frac{\frac{3}{2}\kappa^2}{\tau_D}(R_o/r)^6 \tag{1}$$

where τ_D is the lifetime of D* in the absence of A. The constant R_o depends on the spectroscopic characteristics of the pair; for most systems of interest, it ranges from 2 to 6 nm.[17] The factor $3\kappa^2/2$ is related to the orientation of the transition moments of D* and A. For the case of rapidly reorienting dipoles, the orientationally averaged value of this factor is exactly equal to unity. For most other situations lacking strong orientational correlations, this term falls within 10% of unity.[18] In this work, we will assume $3\kappa^2/2 = 1$.

Two types of energy-transfer experiments have been carried out. In one approach, pioneered by Fayer and co-workers, A = D and one probes the extent of energy migration between identical chromophores (D* to D energy transfer).[19] After one or more migratory steps, the energy is usually dissipated at a trap site. One can determine the rate of this process by measuring the rate of decay of the donor fluorescence intensity, or one can determine the rate of energy transfer by following the rate of donor fluorescence depolarization, assuming complete depolarization in a single transfer step. In the second approach, two different dyes are employed. In this methodology, which is the focus of the work described below, one measures decay of the intensity of the donor fluorescence ($I_D(t)$) in the presence and absence of acceptors. This one-step energy-transfer process is referred to as direct energy transfer (DET).[16]

Imagine a system in which all donors and acceptors are separated by the same distance. Some examples exist for rigid molecules with rigidly attached D and A groups. By measuring the decay rate of the donors, one determines $w(r)$ and is therefore able to calculate the D−A distance r. Since r is already known for the rigid framework, this type of experiment is useful for testing the validity of the theory from which eq 1 is deduced. Most systems of interest are characterized by a distribution of D−A distances. When a sample is excited with a pulse of light, a large ensemble of D* is created. In two types of systems, the various sites occupied by the donors are related by symmetry. In uniformly labeled systems of macroscopic ("infinite") size, such as an extended two- or three-dimensional space, edge effects are unimportant and all donors are related by translational symmetry. In some smaller objects, such as the surface of a sphere or a cylinder, when uniformly labeled, the donors are related by the symmetry of the object. In these situations, one needs to consider only the distribution of A groups around any given D. In other systems, not uniformly labeled, such as polymer interfaces, the donor−acceptor distance distribution also depends on the distribution of D in the sample.

This distribution dependence is the source of the sensitivity for the use of ET experiments to learn about microdomain morphology in polymer systems. $I_D(t)$ is affected by and contains information about the distribution of D−A distances. Through labeling a system by judicial placement of D and A groups in the domain of interest, one hopes to learn about the underlying morphology of the system. To specify completely the morphology of a nanodomain, one would need to obtain information about the composition of the system across the space

of interest. From the knowledge of each component's concentration profile, the "shape" and "size" are completely specified.

Consider a simple example where a DET experiment can provide morphological information about spherical objects. One labels randomly the surface of the core of a micelle[20,21] (or a latex particle[22]) with D and A groups. The concentration profiles of labels now present a description of the system's morphology. The D−A distances are influenced by the radius of the sphere and the local concentration of the A groups (C_A). The distribution function for interdistances of random points on the surface of a sphere is known, and from the methodology developed by Klafter and Blumen (KB),[23a] one calculates the theoretical decay profile[24]

$$I_D(t) = I_D(0) \exp\{-t/\tau_D\} \exp\{-g(t)\} \qquad (2a)$$

$$g(t) = P(t/\tau_D)^{1/3} \qquad P = 4.254 C_A R_o^2 \qquad (2b)$$

In an experiment, one fits the measured $I_D(t)$ decay profile data to eq 2 and recovers P as a fitting parameter. From a spectroscopic knowledge of R_o and the mean number of acceptors (n_A) on each sphere, together with the fact that for the presumed morphology $C_A = n_A/4\pi R_s^2$, one recovers R_s, the size of the sphere. Such an approach was recently utilized in our laboratories to characterize the core of block copolymer micelles.[20] The micelles had $R_s = 7.5$ nm and were shown to have a near smooth surface (on the scale of R_o).

Equation 2, however, cannot be applied to analyze data from a system in which the micelle core is swollen by solvent. This swelling would create a diffuse interface between the core and the solvent, and the dyes distributed around the edge of the core now would become located in a diffuse layer.[21] Under such circumstances, the original KB methodology[23a] requires the knowledge of the *distribution function* for the separation distances of donor−acceptor pairs, which may be difficult to obtain.

There have been several useful approaches to the latter problem, such as representing the surface of a pore by an infinite, cylindrical surface and computing DET between donors and acceptors randomly distributed on it,[23b] or considering the *conformational distribution* of polymer chains labeled by donor and acceptor dyes.[23c] More recently, we have developed a theoretical methodology for calculating $I_D(t)$ decays for *generalized* spatial concentration profiles.[16] The only requirement now is that the concentration profiles follow an element of symmetry, e.g., planar[25] or spherical.[26] For the case of a sample with a plane of symmetry, one has the expression

$$I_D(t) = \exp\{-t/\tau_D\} \int_{-\infty}^{+\infty} C_D(z)\varphi(z, t)\, dz \qquad (3a)$$

$$\varphi(z, t) = \exp\{-g(z,t)\}; \quad w = \frac{1}{\tau_D}(R_o/r)^6 \qquad (3b)$$

$$g(z, t) = 4\pi \int_0^\infty [1 - \exp\{-wt\}] \langle C_A(z, r) \rangle\, r^2\, dr \qquad (3c)$$

$$\langle C_A(z, r) \rangle = \frac{1}{2r} \int_{z-r}^{z+r} C_A(z')\, dz' \qquad (3d)$$

In (3a), z represents the axis along which concentration profiles vary. Because intensity is measured in arbitrary units, we have omitted all proportionality constants of eq 3a. The function $\varphi(z, t)$ measures the probability that an excited donor, positioned on a plane at z, survives the act of energy transfer for the duration of time t. The exponent function $g(z, t)$ and

CHART I

the mean acceptor concentration $\langle C_A(z, r) \rangle$ are defined to simplify the presentation. Physically, $4\pi r^2\, dr\langle C_A(z, r) \rangle$ may be interpreted as the mean number of acceptors within a shell of radius r and thickness dr surrounding a donor positioned on a plane at z. In (3d), the profile $C_A(z')$ must be in units of number density. To calculate $I_D(t)$, the information needed is the spatial dependence of concentration profiles $C_D(z)$ and $C_A(z)$, features determined by the local morphology.

Over the past several years our laboratory has synthesized various block copolymers specifically labeled with a single donor or acceptor chromophore. We have prepared poly-(styrene-*b*-methyl methacrylate) (PS−PMMA) and poly(isoprene-*b*-methyl methacrylate) (PI−PMMA) labeled at the junction.[10,11] We have also prepared similar polymers labeled at the PMMA end.[27] For our DET experiments, the donor chromophore of choice has been phenanthrene. Excited phenanthrene has a relatively long natural lifetime ($\tau_D = 44-46$ ns); but more important, the unquenched decay rate is relatively insensitive to its local environment. For this reason, the unquenched decay is often a simple exponential, facilitating analysis of the fluorescence decay profiles. In experiments, phenanthrene can be excited in the region of 290−300 nm, and its emission is monitored in the region of 350−370 nm. An appropriate acceptor of energy for phenanthrene is the anthracene moiety. Its absorption is weak at 300 nm but strong in the wavelength range ($\epsilon^{max} \approx 10^4$ M^{-1} cm^{-1}) where phenanthrene emits. Its own emission is above 380 nm.

Chart 1 shows an architectural representation of the junction-labeled PI−PMMA. A similar drawing can be made for PS−PMMA. The characteristic feature of interest to us is the difference in the thickness of the interface of these two block copolymers as defined by the distribution of the junction points.

Block Copolymer Morphology

In the bulk state at equilibrium, the two immiscible components of an A−B diblock copolymer self-assemble into a periodic structure.[2,3] Lamellar structures are formed if the sizes of the two blocks are similar. Figure 1a depicts this lamellar structure and indicates the parameters that characterize its morphology. The morphology is characterized by the parameters $H = h_A + h_B$ and δ. H is the period length over which the structure repeats, and δ is a measure of the interface thickness. Finer details of the morphology are determined by the profile across space of the segment density of each block (volume fractions $\phi_B(z)$ and $\phi_A(z)$) and the junction-point distribution ($P_J(z)$). Hypothetical examples of the profiles are shown in Figure 1b.

Scattering and neutron reflectivity experiments provide information about lamellar structures consistent with the picture shown in Figure 1. NR experiments in particular allow $\phi_i(z)$ (i = A, B) to be determined if one fits the experimental data to a model profile. Note that if the copolymer is labeled at the junction, the donor and acceptor dyes occupy the interfacial domain. It is evident that the D−A distances are controlled both by the local number density of acceptors and by the distribution of junction points across the interface. Information
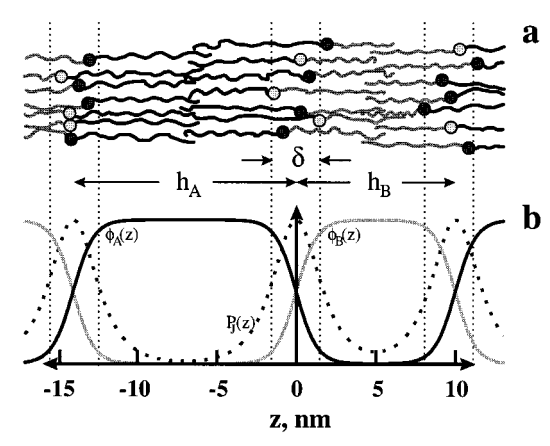
Analysis of Nanoscale Morphologies in Polymers

J. Phys. Chem. B, Vol. 102, No. 41, 1998 **7963**

Figure 1. (a) Schematic representation of microphase separation by A−B diblock copolymer chains into a lamellar morphology. Each junction point is labeled by either of a donor (○) or acceptor (●) dye. The dyes concentrate at the interface. (b) Example of calculated profiles of block volume fractions (ϕ_A and ϕ_B) and the junction distribution function ($P_J(z)$) across a section of the model, using the Helfand−Tagami relations, with parameters approximating the case of PI−PMMA, cf. Table 1. Period spacing length $H = h_A + h_B = 24$ nm; interface thickness $\delta = 2.6$ nm.

about $P_J(z)$, previously unavailable, can in principle be obtained through DET experiments on these systems.

Because of the important bearing system parameters have on one's ability to distinguish the finer details of various morphologies, one needs to pay close attention to the way they are defined. The definition of H is straightforward and can be inferred by reference to Figure 1. If the interface-to-interface (midpoints) distance of each block is designated as h_i (i = A, B), then $H = h_A + h_B$. The definition of the interface thickness δ is somewhat arbitrary. A choice often employed is

$$\delta \equiv 1/\Phi'_B(0) \tag{4}$$

where $\Phi'_B(0)$ is the value of the slope at the center of the interface ($z = 0$). By reference to Figure 2 one notes that eq 4 has a simple geometric interpretation. One draws the tangent to the profile of $\phi_B(z)$, at $z = 0$, and extends it to the z axis. The base of the resulting triangle has a width of $\delta/2$. It is evident that different interfaces having differently shaped $\phi_B(z)$ profiles can be characterized by identical values of δ.

Helfand and Tagami,[13] Leibler,[28] Semenov,[29,30] and others have developed mean-field theories that describe the interface morphology of equilibrium microphase-separated A−B block copolymers. The Helfand-Tagami (HT) expression for the segment density is given by

$$\phi_B(z) = \frac{1}{2}(1 + \tanh(2z/\delta)); \quad \delta = 2b(6\chi)^{-1/2} \tag{5}$$

where b is the statistical monomer length and χ is the Flory−Huggins parameter. Assuming constant density, i.e., $\phi_B(z) + \phi_A(z) = 1$, HT also derived a relation between $P_J(z)$ and $\phi_i(z)$, showing that the product $\phi_A\phi_B \propto P_J^2$, where $P_J(z)$ dz yields the probability of finding a junction point between z and $z + $ dz. For a symmetrical interface, $\phi_A(0) = \phi_B(0) = 0.5$, and one obtains

$$\phi_B - \phi_B^2 = \frac{1}{4}(P_J(z)/P_J(0))^2 \tag{6}$$

Choice of a Distribution Function

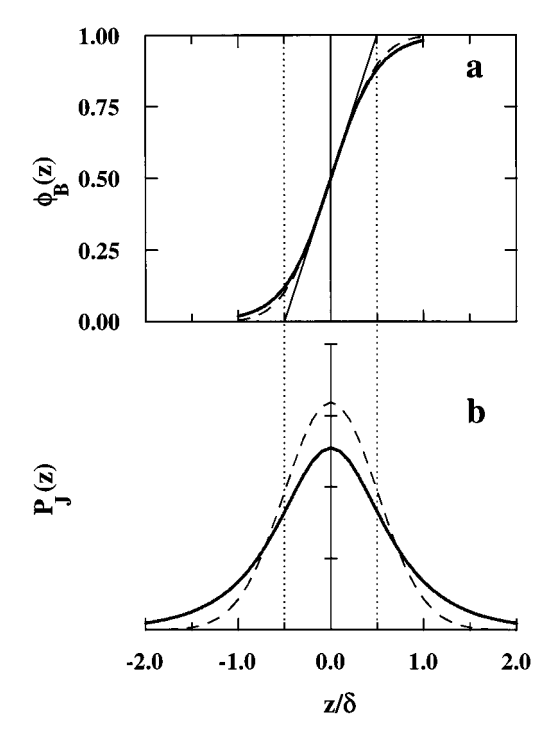One aim of this work is to investigate whether DET experiments on junction-labeled copolymers may be capable

Figure 2. Comparison of two different interface morphologies of equal thickness δ, based on junction distribution functions obtained from the Helfand−Tagami equilibrium theory (solid trace, cf. eq 8) or a hypothetical Gaussian function (dashed trace, cf. eq 9). The corresponding volume fraction profiles are calculated by using eq 6 of the text. Note that the tangent to ϕ_B cuts the horizontal axis at $z = \pm\delta/2$.

of distinguishing the HT junction distribution profile from closely related but fundamentally different profiles. In other words, can DET distinguish between different model profiles? We shall see (cf. eq 8 and Figure 2b) that a general feature of the HT junction distribution is that it is bell-shaped, with wings that decay near exponentially for $|z/\delta| > 1$. The chain ends at the center of an individual lamella are predicted to have a Gaussian distribution.[14] A Gaussian distribution is also bell-shaped and has the form $P_J(z) \propto \exp(-\beta z^2)$, where β is a constant related to δ and is to be determined.[31] To find β we refer to eq 4 as the defining relation. This relation, however, requires knowledge of the volume fraction profile $\phi(z)$ that corresponds to the chosen $P_J(z)$. An arbitrary but logically consistent recourse is to assume that the HT relation (6) between P_J and ϕ_J is also valid for other distributions. In this case, by applying definition (4) to eq 6 we find a new definition for δ, expressed in terms of the junction distribution[32]

$$\delta = 2(-P_J(0)/P_J''(0))^{1/2} \tag{7}$$

where $P_J''(0)$ is the value of the second derivative at $z = 0$. Applying definition (7) to the Gaussian profile and eq 4 to the HT profile (5), we find the two respectively normalized junction distributions[33]

$$P_J(z) = \frac{(2/\pi)}{\delta}\operatorname{sech}(2z/\delta) \qquad \text{Helfand-Tagami (HT)} \tag{8}$$

$$P_J(z) = \frac{(2/\pi)^{1/2}}{\delta}\exp(-2z^2/\delta^2) \qquad \text{Gaussian (G)} \tag{9}$$

Figure 2 shows traces of HT and Gaussian volume-fraction profiles, in addition to the corresponding junction distributions. Note that the HT profile allows a significant fraction of the junction points to exist outside what is defined as the interface

TABLE 1

parameters of simulation	polymer samples	
	PS−PMMA[35]	PI−PMMA[35]
period spacing H, nm	34.5	24.0
interface thickness δ, nm	5.17	2.60
Förster radius R_o, nm[34]	2.3	2.3
donor lifetime τ_D, ns	44	45
acceptor concn C_A, mM	12.9	20.5

thickness (the band within $z = \pm\delta/2$), while the Gaussian has sharper decaying wings. The difference between the corresponding volume-fraction profiles is smaller. Any experiment designed to determine $\phi(z)$ must be very accurate indeed to be able to distinguish the two different morphologies.

For the purpose of DET experiments, one uses a sample labeled at the junctions. Here one expects each local dye concentration profile to be proportional to $P_J(z)$. The proportionality constants may be found from normalization considerations that give[33]

$$C_A(z) = \frac{H\bar{C}_A}{2}P_J(z) \tag{10a}$$

$$C_D(z) = \frac{H\bar{C}_D}{2}P_J(z) \tag{10b}$$

where $\bar{C}_i$ (i = A, D) are the bulk-averaged, experimentally determinable dye concentrations in the sample. In actual practice, one needs to know only $\bar{C}_A$ (in units of number density). Knowledge of $\bar{C}_D$ is not necessary because, as indicated in eq 3a, intensity measurements are made in arbitrary units. Armed with eqs 3 and 8−10, we are now ready to compare the influence of the two closely related morphologies (cf. Figure 2b) on energy-transfer experiments on junction-labeled samples.

Results and Discussion

Simulations provide a powerful methodology for examining the strengths and limitations of an experimental strategy, without the complications of technical difficulties in sample preparation and measurement artifacts. One inputs the structure of the system and the physics of the measurement into the generated data. One then examines the ability of the analytical methodology for recovering the known input parameters. This is one of the few ways in which one can test separately the precision of an experiment and its accuracy.

Here, we simulate lamellar structures formed by junction-labeled diblock copolymers. To proceed, we introduce the morphological parameters, H and δ, and the spectroscopic parameters τ_D, R_o, and $\bar{C}_A$. By specifying δ, we establish through eq 5 the χ parameter characterizing the interaction of the two polymer blocks. We choose the parameters of two lamellar-structure-forming systems, PS−PMMA and PI−PMMA, presented in Table 1. Both represent systems which have been studied previously in our laboratory.[10,11] Russell and co-workers have studied PS−PMMA by neutron reflectivity (NR).[37,38] To put the experimental results in context, in the NR experiments, the magnitude of δ obtained depends on how one corrects for capillary waves at the interface, and the value currently accepted[8] for PS−PMMA is somewhat smaller than the 51 ± 5 Å value originally reported. In our DET experiments on PI−PMMA,[11] we deduced an apparent δ of 26 Å, but this value was obtained without consideration of the shape of the segment density profile across the interface. For the purposes
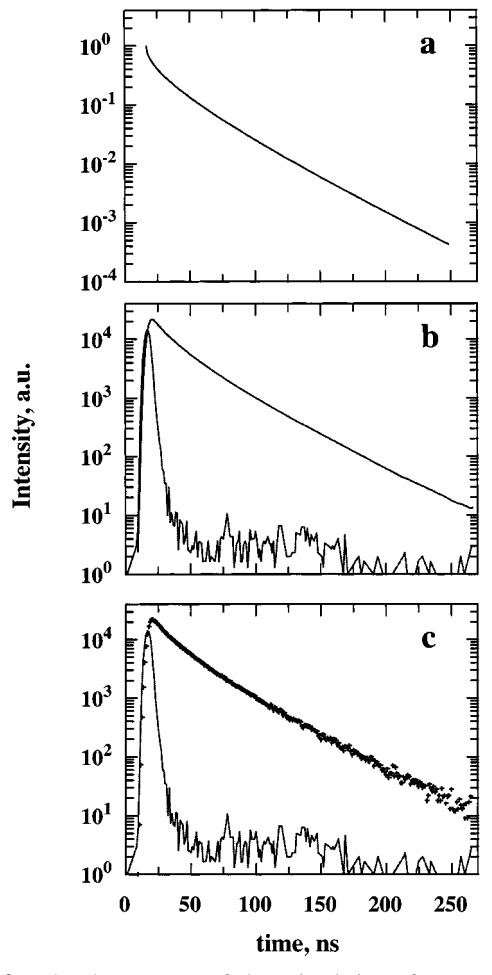

Figure 3. The three stages of data simulation of energy-transfer experiments for a system corresponding to the PI−PMMA sample of Table 1. (a) First, $I_D(t)$ is evaluated numerically (cf. eq 3). (b) Next, the result of part a is convoluted with a real excitation lamp profile ($L(t)$) to yield $I_D^{conv}(t)$. (c) Finally, random Poisson noise is added to the data of part b. For details of the simulation procedure see Appendix A.

of the simulations described here, the values of $\delta = 52$ Å and $\delta = 26$ Å refer to systems that differ in the diffuseness of the interface separating the two components. As a result of the inherent nature of simulation studies, the conclusions of this work will be independent of the close match of the chosen parameters with real experimental systems.

Simulation of Data

In this section, we summarize the generation of simulated data for the single-photon-timing technique,[39,40] deferring some of the more technical details to Appendix A. Three stages are involved in the simulation of experimental data. First, one calculates a time-dependent theoretical excited donor decay profile based upon assumed concentration profiles for D and A. The calculation involves eqs 3, 8 or 9, and 10. Then, one convolutes this survival function with an experimental lamp intensity profile. Finally, one introduces noise in the data, characteristic of a real experiment. An example is presented in Figure 3, which treats input parameters characteristic of PI−PMMA (Table 1) with a Helfand−Tagami junction distribution across the interface (cf. eq 8, Figure 2b). In Figure 3a, we plot the theoretical donor survival profile. The plot would represent the decay if there were no noise, and the excitation source was an ideal delta-pulse (i.e., excitation width $\ll \tau_D$). Next (Figure
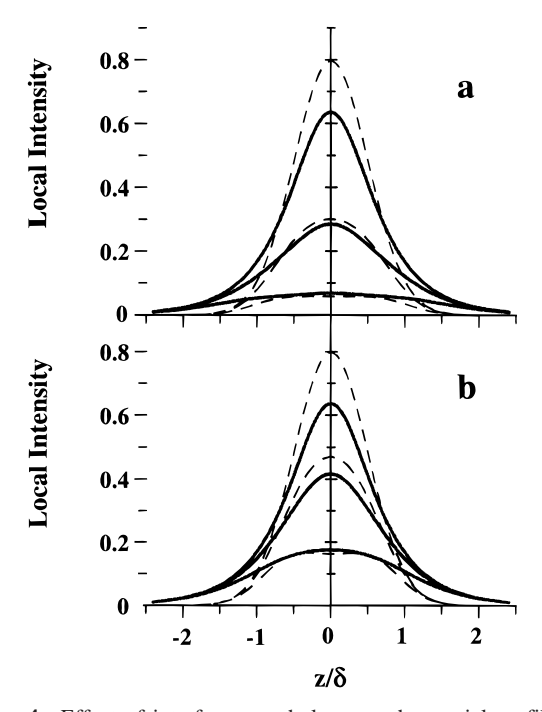
Analysis of Nanoscale Morphologies in Polymers

J. Phys. Chem. B, Vol. 102, No. 41, 1998 **7965**

Figure 4. Effect of interface morphology on the spatial profiles of the local fluorescence intensity (in arbitrary units): (a) PI−PMMA; (b) PS−PMMA of Table 1. In each figure there are three sets of profiles corresponding to, from top-to-bottom, times $t = 0$, $0.1\tau_D$, and $1.0\tau_D$ after pulsed excitation. Solid and dashed traces are for the HT and Gaussian morphologies, respectively. The profiles are calculated from the expression $\exp(-t/\tau_D)C_D(z)\varphi(z,t)$. The profiles, when integrated over the space coordinate z, yield the total donor fluorescence intensity $I_D(t)$ of the text; cf. eq 3a.
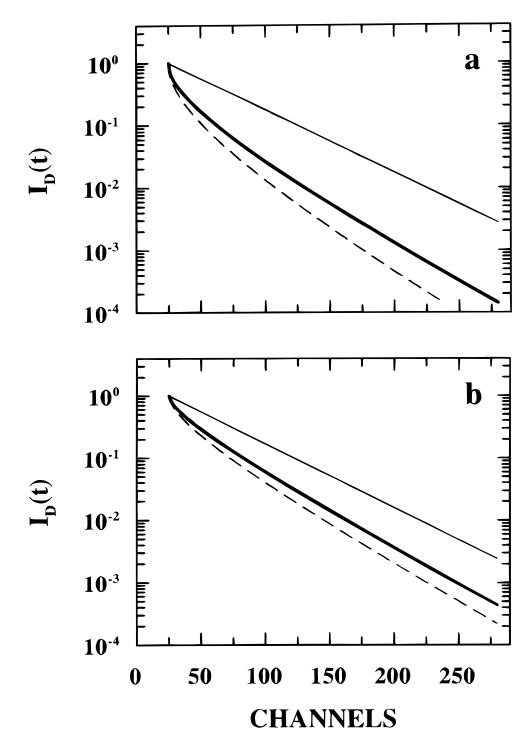

Figure 5. Effect of interface morphology on the calculated temporal profiles of donor fluorescence intensity, in arbitrary units. Solid and dashed traces are for the HT and Gaussian morphologies, respectively. The thin straight line in each plot represents the single-exponential decay of donors in the absence of acceptors. The profiles are calculated for the two samples of Table 1: (a) PI−PMMA; (b) PS−PMMA, using eqs 3 and 8−10. Each channel represents 1.04 ns.

3b), we use an excitation-lamp profile obtained in a real experiment and convolute for the effect of finite excitation pulse width. In the case of the PS−PMMA sample, we also choose to add a simulated component of scattered light. The calculated values are normalized to yield a peak intensity near 20 000 counts. Finally (Figure 3c), we add Poisson noise, which closely simulates the experimentally observed noise of this technique.

While our ultimate goal is to examine the analysis of simulated data in the same way one analyzes experimental data, the simulation also allows one to learn about features of the system inaccessible to experimentation. For example, one can ask about the spatial distribution of donors contributing to the signal at various times following pulsed sample excitation. Important insights into the DET experiment are available through consideration of the *local* donor fluorescence intensity emanating from each element of length across the interface. Mathematically, this can be represented by the integrand of eq 3a, that is, $\exp\{-t/\tau_D\}C_D(z)\varphi(z,t)$. From (3a), it is clear that the total integration of local intensity across the interface yields the observable $I_D(t)$. Figure 4 shows the calculated spatial profiles of the local intensity for the two samples of Table 1. Calculations are made for times $t = 0$ (immediately after excitation), $t = 0.1\tau_D$ (approximately 4.5 ns), and $t = 1.0\tau_D$ (approximately 45 ns). The $t = 0$ profiles represent the actual junction distributions (cf. Figure 2b). The results show that even for very short times ($t = 0.1\tau_D$), there is an appreciable drop of intensity at the center of the interface. This occurs because acceptors are concentrated near the center of the interface. The donors at the junctions of PI−PMMA decay even faster than those of PS−PMMA, because they have a narrower interface (PI−PMMA, $\delta = 2.6$ nm; PS−PMMA, $\delta = 5.2$ nm), thus crowding acceptors into a smaller interfacial volume.

We can also compare the influence of the distribution of junctions on this effect. For two samples characterized by a common value of δ, the Gaussian (dashed traces) and HT (solid traces) morphologies lead to very different donor fluorescence decay profiles. The system with the Gaussian distribution decays faster because there are fewer acceptors in the wings and more near the center. An important lesson we take for future analytical work is that beyond a time of τ_D (for $t > \tau_D$), most of the intensity originates from the wings of the distribution, away from the center of the interface. Consequently, if one is interested in learning about features near the center of the distribution, one should choose a time resolution even shorter than the 0.025τ/channel currently employed in our single-photon-timing experiments.

By integrating the profiles of Figure 4 over z, we arrive at $I_D(t)$. Representative profiles are shown in Figure 5a for PI−PMMA and in Figure 5b for PS−PMMA. Here $I_D(t)$ represents the decay in the absence of noise and convolution by lamp. As in previous figures, the solid lines refer to simulations involving a Helfand−Tagami distribution of junctions and the dashed traces correspond to the Gaussian distribution. Conclusions drawn earlier, from Figure 4, are also valid here: donors decay more rapidly for labeled PI−PMMA than for PS−PMMA because the dyes are confined to a narrower interface. For a given polymer and interface thickness δ, the Gaussian junction distribution leads to a faster decay than the HT distribution, because smaller fractions of the donors and acceptors are distributed in the tails (cf. Figure 2b). In fact, when we first obtained these results, we thought that the energy-transfer experiments might be able to distinguish the two closely related morphologies of equal δ. As we see below, however, this expectation was overly optimistic.
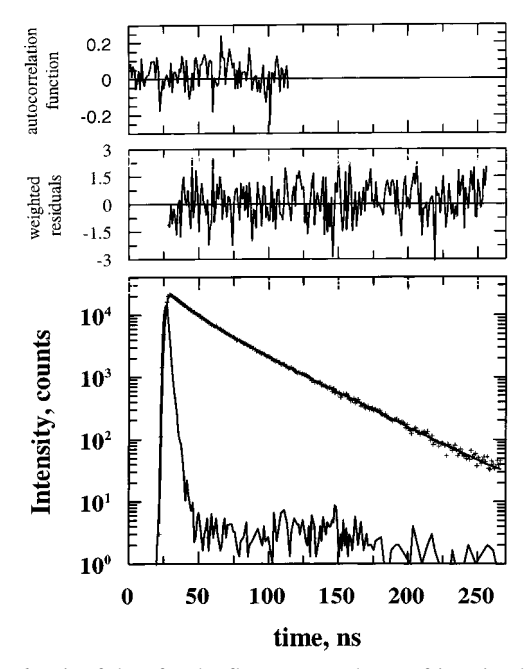
Figure 6. Fit of data for the fluorescence decay of junction-labeled PS−PMMA of Table 1, simulated for a Helfand−Tagami distribution of junctions. A "good" fit ($\chi^2 = 1.10$) is obtained by assuming the correct morphology, even when fixing H to an erroneous value (17.25 nm). The fit recovers an erroneous value of $\delta/R_o = 0.967$ nm. The upper insets show acceptable behavior for the time dependence of the residuals and autocorrelation function (see Appendix B).

Analysis of Data

In this section, we analyze the simulated data as though they were generated in real experiments. Technical details of the procedure are explained in Appendix B. Figure 6 shows the typical result of a simulated phenanthrene donor decay, with a trace of the calculated best fit drawn through the data points. In the analysis, we assume prior knowledge of the independently measurable spectroscopic parameters R_o, $\bar{C}_A$; and τ_D and take them to be those given in Table 1. The χ^2 quality-of-fit measure is the primary criterion used for identifying the "best" fit. There are three fitting parameters. One is the initial intensity value, which we denote by A. It depends mainly on the number of counts collected in the experiment rather than being characteristic of the material. The two other fitting parameters in our analysis are $H\bar{C}_AR_o^2$ and δ/R_o, related to the material parameters H and δ through the known value of the spectroscopic length scale, R_o. The best possible fit is obtained when the deviation between the simulation and the calculated fit in each data channel corresponds to the Poisson noise only. In this case, $\chi^2 = 1.0$. Otherwise, χ^2 tends to be greater than unity. From past experience, with regard to analysis of real experimental data, we can describe the quality of a fit as follows:[41] very good, if $\chi^2 \leq 1.1$; good, if $1.1 < \chi^2 \leq 1.2$; acceptable, if $1.2 < \chi^2 \leq 1.5$; unacceptable, if $\chi^2 > 1.5$. A bad fit implies either that one has assumed the wrong morphology, i.e., the wrong function describing the junction distribution, or that the parameters obtained from the fit deviate from those of the actual system. As in all experiments in which one fits data to a model, an incorrect choice of a model can still result in statistically acceptable fitting parameters. A good fit to the data by itself does not prove the model morphology or the validity of the recovered fitting parameters.

Parameter Optimization

Figure 6 shows a typical donor fluorescence decay, obtained in the simulation of the PS−PMMA sample of Table 1, that obeys the Helfand−Tagami morphology. The fit to the data is also shown, for a situation presuming the HT morphology. The first issue we address concerns the analytical limits in recovering the morphological parameters H and δ, assuming that we use the correct model for the junction-distribution profile across the interface. In Figure 6, the data were simulated for the junction-labeled PS−PMMA sample with a Helfand−Tagami distribution having the material properties described in Table 1. In the analysis of data, we first assume that we know that the system is characterized by a Helfand−Tagami distribution. There are three fitting parameters and three different strategies one can envision for the data analysis, depending upon how many of these parameters are known independently. In the most general approach, we can ask the fitting program to seek the best fit for all three parameters. While for some experiments fluorescence decay profiles can be fitted successfully to three or even four unique fitting parameters, this general analysis fails here. For the simulations examined, we commonly find a wide range of H and δ values for which the fits are good ($\chi^2 \leq 1.1$), and one cannot distinguish among them. We *must* possess auxiliary information.

A second strategy involves fixing the value of H, presuming that it can be determined independently through, for example, a scattering experiment. One then asks the fitting program to vary both A and δ, to minimize χ^2, and to provide the best estimate of both δ and A. Finally, in an alternative procedure, one can obtain the optimum value of these two parameters by fixing the value of H, fix-estimating a value of δ, and using the fitting program to vary A, minimizing χ^2. In this way, each decay curve is fit to only one variable parameter. One then repeats this operation for various estimates of δ and constructs a plot of δ vs χ^2, seeking the δ value for which χ^2 is a minimum.

The "second strategy" mentioned in the previous paragraph would require partial derivatives with respect to the model parameter δ/R_o. We elected a computationally simpler approach: fixing δ/R_o and minimizing χ^2 with respect to A and H. However, we then encountered difficulties discussed in more detail below: strong correlation between the model parameters H and δ. The bottom curve of Figure 7 shows that very low χ^2 values can be obtained for a wide range of interface thicknesses, if we allow the least-squares minimization program to adjust H. A simple solution was to minimize only with respect to the parameter A, as described in the second half of the preceding paragraph. Figure 7 shows that the latter approach generates steep χ^2 surfaces. In the curve shown, the minimum of the χ^2 surface lies at $\chi^2 = 1.07 \pm 0.05$ and $\delta/R_o = 1.13 \pm 3\%$, close to the value expected for the sample. The reproducibility of the results is estimated by using different random number streams for the generation of the Poisson noise of the simulations (Figure 9). Not shown in Figure 7 are the data for the PS−PMMA sample, which behaves similarly. Here, by fitting the decay profiles to the single parameter A for a range of fixed values of δ, one recovers the best estimate of the interface thickness at $\chi^2 = 1.07 \pm 0.03$ and $\delta/R_o = 2.27 \pm 0.5\%$, in close agreement with the sample characteristics used in the simulation (cf. Table 1).

At this point, one may draw the conclusion that reliable estimates of the interface thickness δ can be obtained if one has prior knowledge of the morphology and the value of the period spacing H. The question naturally arises as to what happens if one's prior knowledge of H is in error. Figure 8 shows an analysis of the PS−PMMA data starting with erroneous estimates of H. Dependent on the fixed value of H, different χ^2 surfaces are generated, the minima of which yield

Analysis of Nanoscale Morphologies in Polymers

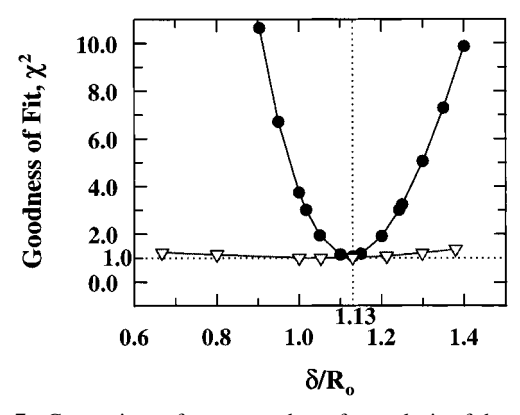*J. Phys. Chem. B, Vol. 102, No. 41, 1998* **7967**

Figure 7. Comparison of two procedures for analysis of data. Filled circles (●) represent cases in which each data point is obtained from a fit of the decay profile to a single fitting parameter. For each point plotted, H is fixed at its true value and δ is fixed at an estimated value. The fitting program varies the initial intensity value (A) to obtain the minimum χ^2 shown. This operation is then repeated for other fixed estimates of δ. Empty triangles ($\triangledown$) represent the potential difficulties of data fitting. Strong correlations between the model parameters H and δ can lead to erroneous conclusions; a wide range of (H, δ) pairs are consistent (χ^2 well below 1.5) with the same fluorescence decay curve. (See the discussion of Figures 8 and 9.) The original fluorescence data were simulated for the junction-labeled PI−PMMA of Table 1 with a Helfand−Tagami morphology. Positions for the true value of δ/R_o (1.13) and optimum χ^2 (1.0) are indicated by dotted lines. For more details see Appendix B.
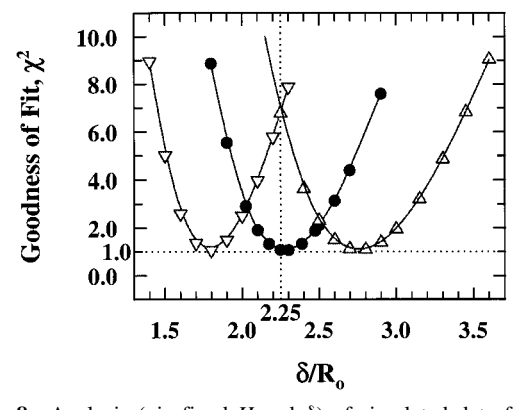

Figure 8. Analysis (via fixed H and δ) of simulated data for PS−PMMA (Table 1) with a Helfand−Tagami morphology. Comparison of the χ^2 surfaces obtained for fixed (true and erroneous) input values of the period spacing H. From left to right: ($\triangledown$) represents $H = 27.6$ nm (80% of the true value); (●) represents $H = 34.5$ nm (the true value); ($\triangle$) represents $H = 41.4$ nm (120% of the true value). The analysis presumes the correct interface morphology. Positions of the true value of δ/R_o (2.25) and optimum χ^2 (1.0) are indicated by dotted lines.

the statistically optimum (but erroneous) estimates of δ/R_o. An example of such a fit was seen in Figure 6. It is apparent that underestimation of H leads to a corresponding underestimation of δ. The correlation of the data suggests that H/δ might be a more appropriate fitting parameter. Figure 9 shows an investigation of the correlation between the error in the presumed value of H fixed in the data analysis and the error in the recovered ratio of H/δ.

First, we note that if H is known fairly accurately so that its assumed value is accurate to ±20%, then the values of H/δ are recovered quite precisely, essentially with zero error for the PS−PMMA "samples". The PI−PMMA samples are more sensitive, and these analyses start showing small discrepancies as soon as H is underestimated to a significant extent (Figure 9). The reasons for this behavior are not difficult to understand if we
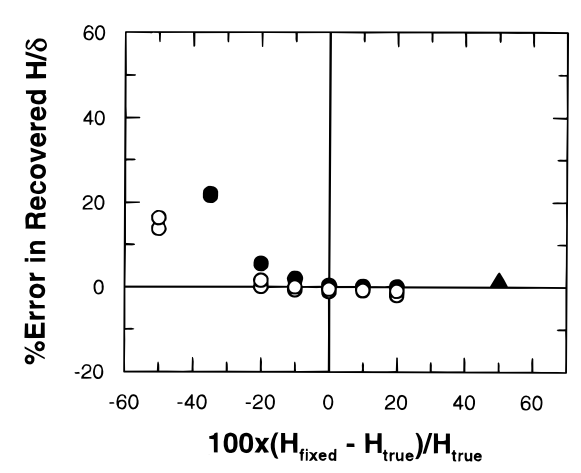

Figure 9. Analysis of the data corresponding to PI−PMMA (●, ▲) and PS−PMMA (○) with a Helfand−Tagami junction profile. In each analysis, H is fixed either at its true value or at a different value and δ is recovered from the optimal position of the χ^2 curve, as shown in Figure 8. The percent error in the recovered H/δ (relative to the corresponding value from Table 1) is then plotted as shown. The vertical scatter of data points represents reproducibility of the results using different random number streams in the generation of the Poisson noise. (Deconvolutions were always conducted on duplicate simulated decay curves, but often the duplicate results were so close that they are not visible or hardly visible in the figure.) The ▲ symbols for PI−PMMA call the reader's attention to the fact that although the H/δ values obtained were accurate, the least-squares analyses results were unacceptable. The minimum χ^2 values were too high, and in particular, the autocorrelation functions clearly indicated that the assumed model parameters were wrong.

examine transformed versions of eqs 3c and 3d, as applicable to the Helfand−Tagami junction distribution

$$g(\zeta, t) = H\bar{C}_A R_o^2 \int_0^\infty [1 - \exp\{-wt\}]F_A(\zeta, \rho)\rho^2 \, d\rho \quad (11a)$$

$$F_A(\zeta, \rho) = \frac{1}{\rho} \int_{\zeta-(2R_o/\delta)\rho}^{\zeta+(2R_o/\delta)\rho} \text{sech}(\zeta') \, d\zeta' \quad (11b)$$

where $\zeta = 2z/\delta$, $\zeta' = 2z'/\delta$, and $\rho = r/R_o$.

We note that increasing H augments the value of $g(\zeta, t)$ for all values of ζ and t, whereas increasing δ lowers its value by narrowing the range of integration with respect to ζ'. It appears that the least-squares minimization process is very efficient in the neighborhood of the "true" value of H, and we can obtain excellent fits to the simulated data by taking advantage of this correlation, recovering the correct H/δ ratio. However, if our knowledge of H is rudimentary, then we have to contend with difficulties of two different nature:

One is that for narrow Helfand−Tagami interfaces eqs 3 and 11 approach the fluorescence decay formula corresponding to an isotropic mixture of donors and acceptors on an infinite two-dimensional surface, similar to that derived by Hauser and co-workers:[42]

$$I_D(t) = \exp[-(t/\tau_D)] \exp[(-g_2(t)] \quad (12a)$$

$$g_2(t) = \frac{\pi}{2} H\bar{C}_A R_o^2 \left(\frac{t}{\tau_D}\right)^{1/3} \Gamma\left(\frac{2}{3}\right) \quad (12b)$$

Then, the correlation between H and δ breaks down, and we recover an incorrect H/δ ratio. This is shown in Figure 9. We also see that this effect takes place sooner for the narrower interface of PI−PMMA than for the thicker PS−PMMA interface.
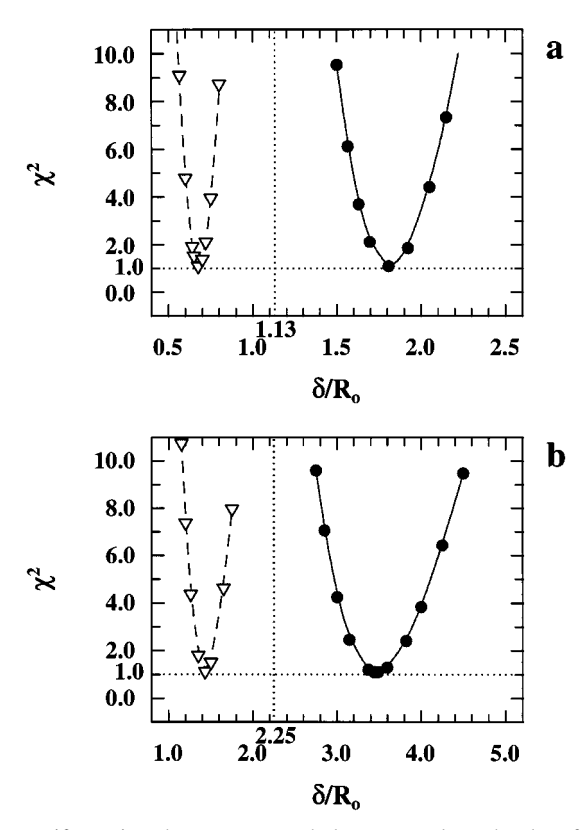
7968 *J. Phys. Chem. B, Vol. 102, No. 41, 1998*

Yekta et al.

Figure 10. Using the wrong morphology to analyze the data from samples of Table 1, (a) PI−PMMA and (b) PS−PMMA. Data corresponding to each sample were generated by either an HT interface distribution (solid traces) or a Gaussian distribution (dashed traces). Next, the data were analyzed with the presumption of the opposite distribution. In all cases, the correct value of H is introduced into the analysis and an incorrect value of δ/R_o is obtained. The positions of the true value of δ/R_o and optimum χ^2 are indicated by dotted lines.

If the assumed value of H is much too high, then a different situation arises. We note from the triangle symbols identifying this case that χ^2 minimization appears to have yielded the correct H/δ ratio, but this is illusory. In fact, the minimum χ^2 value obtained in the two computations represented there was 1.495 (much higher than for the other points shown in Figure 9), and the autocorrelation plots clearly showed that the fits were not acceptable. It appears that single-photon-timing experiments can rule out erroneous values of the lamellar period spacing— if they are too high, and if we are, indeed, dealing with Helfand−Tagami junctions. (We have not conducted a similar investigation for Gaussian junctions.)

Typical values of H are in the tens of nanometers; they may be determined with confidence from scattering experiments. The preceding analysis suggests that it will then also be possible to determine the interface thickness (via H/δ) by DET experiments, without significant loss of precision. Indeed, if for any reason H has been considerably overestimated from the scattering experiments, single-photon-timing measurements will indicate the error. On the other hand, if the erroneous H values are much too *low*, DET will not detect this; rather, it will provide interface thickness results that are also incorrect.

Model Discrimination

The second issue we wish to address is whether in the absence of knowledge about the interface morphology it will be possible to simultaneously determine the interface thickness and the junction distribution profile. Figure 10 shows what happens if one analyzes the data with the wrong type of interface
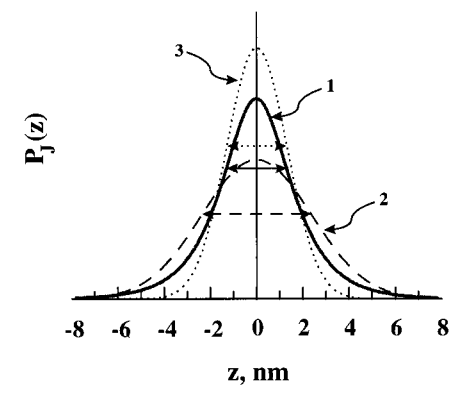

Figure 11. Normalized distribution functions for the parameters of Figure 10a. Curve 1, solid line: Data were simulated using the HT distribution with an interface thickness $\delta = 2.6$ nm ($\delta/R_o = 1.13$). Curve 2, dashed line: The fit of the data to a decay in an interface with a Gaussian distribution of junction points yields an optimum fit for $\delta = 4.7$ nm ($\delta/R_o = 1.81$). Curve 3, dotted line: For the sake of comparison, a Gaussian distribution with $\delta = 2.6$ nm is also shown. Double-headed arrows show the interface thickness of each distribution.

morphology. In Figure 10a, the solid trace depicts the case where the PI−PMMA sample of Table 1 is characterized by a Helfand−Tagami interface distribution, but the fluorescence data are analyzed assuming a Gaussian distribution with the prior knowledge of the correct value of H. One notes that the "best fit" recovers a value of δ that is about 60% larger than the true value. The dashed trace of Figure 10a shows the inverse situation, where the sample is simulated following a Gaussian profile but analyzed assuming a HT morphology. In this case, the program recovers a best-fit estimate of δ considerably lower than the true value. Figure 10b indicates that the PS−PMMA sample of Table 1 shows the same behavior. Clearly, assuming an incorrect description of the interface structure leads to an incorrect estimate of δ. From the comparison of the two junction distribution profiles in Figure 2b, we may see what is happening. For equal values of δ, the Gaussian distribution leads to a faster fluorescence decay (cf. Figures 4 and 5). When the originally HT data are forced to fit a Gaussian-type interface, the fitting program compensates for the lower efficiency of energy transfer with a higher estimate of δ. Similar conclusions may be drawn for the other traces of Figure 10.

The astute reader will recall that δ is defined somewhat arbitrarily for the Gaussian and HT distributions. Thus, it becomes worthwhile to compare the junction distributions themselves for the fit of the data to the correct and incorrect distribution functions. In Figure 11 we plot $P_J(z)$ versus z for three cases. The solid line, labeled 1, represents the HT distribution of the simulation. The dashed line, labeled 2, represents the "best fit" to a Gaussian distribution. This distribution is considerably broader at its half-width than the simulated HT distribution and is significantly less peaked. A Gaussian distribution with the same interface thickness δ as the HT distribution (curve 3 in Figure 11) would be even more sharply peaked with a smaller fraction of the donors and acceptors in the tail of the distribution. It is apparent that a change in the definition of δ will not resolve the problem.

Conclusions

Simulations of energy-transfer kinetics were carried out for a lamellar block copolymer system in which donor and acceptor dyes were attached to the block junction. In such a system, the distribution of donors and acceptors follows that of the junctions across the interface ($P_J(z)$). Assuming that one has

Analysis of Nanoscale Morphologies in Polymers

J. Phys. Chem. B, Vol. 102, No. 41, 1998 **7969**

prior knowledge of the form of this distribution function, as, for example, from a theory of block copolymers, energy-transfer experiments can lead to reliable estimates of the ratio of period spacing to interface thickness (H/δ) but not the individual parameters H and δ. Because reliable values of H can be determined by scattering and/or other techniques, δ may be determined with better than 5% accuracy. Attempts to distinguish a Helfand–Tagami profile from a Gaussian profile were not successful. An energy-transfer experiment may be employed to reject the wrong morphology only if prior values of H and δ are determined by other methods.

It may be possible to improve on these conclusions by extending the measurements to shorter times, where the experiment is particularly sensitive to the peak of the $P_J(z)$ distribution, and to implementation of global analysis[48] for a series of experiments involving a range of acceptor concentrations.

Attempts to fit real experimental data to eq 3 with a Helfand–Tagami junction distribution have met with mixed success. These results will be reported separately. We would like to point out two types of problems that could frustrate analysis of this type of data, one technical and the other of fundamental scientific significance. As an example of the first type of problem, we cite the possibility that the polystyrene component in PS–PMMA has a weak absorption tail extending out into the wavelength region where phenanthrene is excited. Competing emission from PS would distort the fluorescence decay, especially at $t < 10$ ns. More interesting is the possibility that deviations from a good fit in terms of eq 3 are due to a second distribution of junctions in the plane of the interface. The analysis described above presumes a uniform distribution of junctions in the x–y plane. With current technology, the only way to know if there are correlations of the position of the junction points in this plane is through theory or molecular simulation.

Appendix A

The first stage of the simulation involves numerical calculation of $I_D(t)$ in eq 3, e.g., calculation of the trace in Figure 3a. For both Gaussian and Helfand–Tagami distributions (cf. eqs 8–10), eq 3d leads to well-known analytic functions. To evaluate eq 3c, means were developed to deal with the improper integrals. One difficulty is the sharp peak in the integrand that results from an initial parabolic increase, followed by "tailing". For this reason and although [3d] leads to analytic functions for $\langle C_A(z, r) \rangle$, we chose to approximate the integrals in $\langle C_A(z, r) \rangle$ by cubic Taylor polynomials for $z \pm r$ near zero and by their asymptotic limits for $z \pm r \to \pm\infty$. This has the advantage that the integrals of eq 3c become expressible in terms of incomplete γ functions. Numerical integration (Gaussian quadrature) was employed only for the correction terms arising from the approximations. For the final evaluation of the improper integral of eq 3a, we used standard techniques of truncation (for the Gaussian distribution) and logarithmic transformation (for the Helfand–Tagami distribution), prior to (this second set of) Gaussian quadratures. The rules employed were 61-node Gauss–Kronrod quadratures QK61, essentially as implemented in ref 43, but modified for faster execution, as suggested in ref 44. From the difference between the 30-node Gauss and 61-node Kronrod rules, we estimate that a precision of 10^{-6} or better was attained in the numerical quadratures; we

were setting the same error bound for other approximations involved in the computational schemes.

The second stage of simulation requires convolution of the above calculated $I_D(t)$ for the effect of a real experimental excitation lamp, e.g., the calculation of the trace in Figure 3b. An actual excitation-lamp function ($L(t)$), uninfluenced by the measuring system's response, cannot be determined directly.[39,40] We first measured a "mimicked" experimental lamp function ($L_{mim}(t)$) by exciting a solution of p-terphenyl and observing its fluorescence ($\tau = 0.96$ ns) in aerated cyclohexane. $L(t)$ was subsequently calculated (the "demimicking" operation) from the deconvolution relation

$$L_{mim}(t) = \int_0^t L(t') \exp\{-(t - t')/0.96\} \, dt' \qquad (A1)$$

Because the dye is short-lived and 0.96 ns is much less than the lamp width at its half height ($\sim$6 ns), $L(t) \approx L_{mim}(t)$. Next, the lamp-convoluted theoretical decay profile ($I_D^{conv}(t)$) was calculated using the convolution relation

$$I_D^{conv}(t) = A \int_0^t L(t') I_D(t - t') \, dt' \qquad (A2)$$

where A is a normalizing constant that adjusts the initial intensity and $I_D(t)$ is the numerically calculated value of eq 3a described above. The numerical integrations of eq A2 employed a simple trapezoidal rule. In cases where scattered light was added, it was taken as 20% of $L(t)$.

The final stage of simulation requires addition of Poisson noise. For each time channel t_i ($i = 1-256$), the simulated intensity ($I_D^{sim}(t_i)$) is obtained by simply adding the noise to the convoluted data ($I_D^{conv}(t_i)$) described above. Random number generation and conversion to Poisson integer variates were performed according to documented procedures.[45] The standard deviation of the Poisson noise equals (signal counts)$^{1/2}$ at each time channel, going from about 1% at the peak of 20 000 counts, to about 15% for a final intensity value of 50 counts. Repeat simulations of the same fluorescence decay curve were conducted (based on different random number streams).

Appendix B

The general procedure for the calculation of the best-fit intensity is as follows. For a given presumed morphology and each time channel t_i ($i = 1-256$), an estimate of the fitting intensity ($I_D^{fit}(t_i)$) is made by calculating the expression $I_D^{fit}(t_i) = AF_i(t_i/\tau_D, \bar{C}_A, \delta/R_o, H\bar{C}_A R_o^2)$ where F_i is the lamp-convoluted form of eq 3a (see Appendix A, eq A2) and A is a parameter that adjusts the initial intensity. This is exactly what is done to calculate $I_D^{conv}(t)$ for the simulations. The difference is that, in the simulation, all parameters are taken from Table 1, and A is chosen as a number to obtain approximately 20 000 counts at maximum intensity. In the fitting procedure, only the values of τ_D, $\bar{C}_A$, and R_o are presumed known and taken from Table 1. The other parameters A, H, and δ are guessed at. The estimation of A is always done by the program for finding the best fit. The estimations of H and δ can also be done by the program. However, for reasons discussed in the text, if we require the fitting program to find the best fit by freely varying A, H, and δ, we do not find reliable results. Therefore, H and δ are guessed at by the user of the program and input as fixed values in the calculation of $I_D^{fit}(t_i)$. Next, the program evaluates the weighted difference between simulation and fit (weighted residual R)

$$R(t_i) = (I_{\mathrm{D}}^{\mathrm{sim}}(t_i) - I_{\mathrm{D}}^{\mathrm{fit}}(t_i))/(I_{\mathrm{D}}^{\mathrm{sim}}(t_i))^{1/2} \qquad \text{(B1)}$$

for each channel i, and from this, one calculates the χ^2 value of the fit using the expression

$$\chi^2 = \frac{1}{(257 - n - i^*)} \sum_{i=i^*}^{i=256} R_i^2 \qquad \text{(B2)}$$

Here, i^* equals the channel number where the fitting starts (typically, i^* equals the channel of peak fluorescence intensity) and n is the number of fitting parameters the fitting program varies to minimize χ^2. If only A is varied, then $n = 1$; if A and δ are varied, $n = 2$; etc. For each set of the estimated values of H and δ, the program finds the value of A and the corresponding minimized value of χ^2. When $n = 1$, we use a simple linear regression algorithm. When $n > 1$, we use the Levenberg–Marquadt procedure, as implemented by Moré et al.[46] If the estimates of H and δ happen to be those in Table 1 (i.e., those used in the simulations), then $I_{\mathrm{D}}^{\mathrm{fit}}(t_i) \approx (I_{\mathrm{D}}^{\mathrm{sim}}(t_i) -$ (Poisson noise)$_i$) and it follows that $\chi^2 \approx 1.0$. Otherwise, χ^2 tends to be greater than unity. The autocorrelation function of residuals, $C(t)$, is evaluated from the expression $C(t_j) \propto \sum_{i=i^*}^{i=256-j} R(t_i)R(t_{i+j})$, where $R(t)$ was defined in eq B1. The proportionality constant is found by requiring $C(0) = 1$. A nonrandom distribution of C-points or of the residuals $R(t_i)$ about zero is indicative of a bad fit. In some cases, the former behavior shows up even when χ^2 is approximately equal to 1.0. This is presumed to signify a fit of data to the wrong model.[47] We have not observed this behavior for the fit of our simulated morphology data to the wrong models (cf. Figure 6), only in some cases where we specified erroneous H values (cf. Figure 9).

References and Notes

(1) Paul, D. R., Newman, S., Eds. *Polymer Blends*; Academic Press: San Diego, 1978.

(2) Fredrickson, G. H.; Helfand, E. *J. Chem. Phys*. **1987**, *87*, 697.

(3) Bates, F. S.; Fredrickson, G. H. *Annu. Rev. Phys. Chem*. **1990**, *41*, 525.

(4) Stamm, M.; Schubert, D. W. *Annu. Rev. Mater. Sci*. **1995**, *25*, 325.

(5) Russell, T. P. *Physica B* **1996**, *221*, 267.

(6) Russell, T. P. *MRS Bull*. **1996**, *21*, 49.

(7) Schubert, D. W.; Stamm, M. *Physica B* **1997**, *234–236*, 286.

(8) Sferrazza, M.; Xiao, C.; Jones, R. A. L.; Bucknall, D. G.; Webster, J.; Penfold, J. *Phys. Rev. Lett*. **1997**, *78*, 3693.

(9) Fredrickson, G. H. *Macromolecules* **1986**, *19*, 441.

(10) Ni, S.; Zhang, P.; Wang, Y.; Winnik, M. A. *Macromolecules* **1994**, *27*, 5742.

(11) Tcherkasskaya, O.; Ni, S.; Winnik, M. A. *Macromolecules* **1996**, *29*, 610.

(12) Farinha, J. P. S.; Martinho, J. M. G. *J. Lumin*. **1997**, *72–74*, 914.

(13) Helfand, E.; Tagami, Y. *J. Chem. Phys*. **1972**, *56*, 3592.

(14) Rubinstein, M.; Obukhov, S. P. *Macromolecules* **1993**, *26*, 1740.

(15) Förster, Th. *Ann. Phys*. **1948**, *2*, 55.

(16) Yekta, A.; Winnik, M. A. In *Solvents and Self-Organization of Polymers*; Webber, S. E., Munk, P., Tuzar, Z., Eds.; Kluwer: Dordrecht, 1996; pp 433–455.

(17) Berlman, I. B. *Energy Transfer Parameters of Aromatic Compounds*; Academic Press: New York, 1973.

(18) See ref 16 and the references therein.

(19) Peterson, K. A.; Stein, A. D.; Fayer, M. D. In *Molecular Dynamics in Restricted Geometries*; Klafter, J., Drake, J. M., Eds.; John Wiley and Sons: New York, 1989; pp 77–98.

(20) Schillén, K.; Yekta, A.; Ni, S.; Winnik, M. A. *Macromolecules* **1998**, *31*, 210.

(21) Duhamel, J.; Yekta, A.; Ni, S.; Khaykin, Y.; Winnik, M. A. *Macromolecules* **1993**, *26*, 6255.

(22) Charreyre, M. T.; Yekta, A.; Winnik, M. A.; Delair, T.; Pichot, C. *Langmuir* **1995**, *11*, 2423.

(23) (a) Klafter, J.; Blumen, A. *J. Chem. Phys*. **1984**, *80*, 875. (b) Levitz, P.; Drake, J. M.; Klafter, J. *Chem. Phys. Lett*. **1988**, *148*, 557. (c) Roy, A. K.; Blumen, A. *Physica D* **1989**, *38*, 291.

(24) Levitz, P.; Drake, J. M.; Klafter, J. *J. Chem. Phys*. **1988**, *89*, 5224.

(25) Yekta, A.; Duhamel, J.; Winnik, M. A. *Chem. Phys. Lett*. **1995**, *235*, 119.

(26) Yekta, A.; Winnik, M. A.; Farinha, J. P. S.; Martinho, J. M. G. *J. Phys. Chem*. **1997**, *101*, 1787.

(27) Ni, S.; Sakamoto, N.; Hashimoto, T.; Winnik, M. A. *Macromolecules* **1995**, *28*, 8686.

(28) Leibler, L. *Macromolecules* **1980**, *13*, 1602.

(29) Semenov, A. N. *Sov. Phys. JETP* **1985**, *61*, 733.

(30) Semenov, A. N. *Macromolecules* **1993**, *26*, 6617.

(31) The Gaussian distribution occurs in many physical systems where the events are statistically independent. This is not expected of a junction point whose placement is influenced by local composition of the neighboring chains.

(32) The derivation follows because we are interested in the region as $z \to 0$. Here we write $P_{\mathrm{J}}(z) = P_{\mathrm{J}}(0) + P_{\mathrm{J}}''(0)z^2/2 + ...$, remembering that at the maximum of $P_{\mathrm{J}}(z)$, $P_{\mathrm{J}}'(0) = 0$. Substitution in eq 6, followed by application of eq 4 yields the desired result.

(33) Normalization yields the proportionality factors of eqs 8 and 9 by considering that the probability of finding a junction point somewhere along the z axis is unity. That is, $\int_{-\infty}^{+\infty} P_{\mathrm{J}}(z)\, \mathrm{d}z = 1$. Correspondingly, integration of eq 10a along the z axis and over a $1 \times 1\ \mathrm{cm}^2$ cross-sectional area, gives the total number of acceptors in 1 cm^3 of the sample (i.e., $\bar{C}_{\mathrm{A}}$). The factor $H/2$ comes in because there are two interfaces per period length and $1/H$ interfaces per centimeter of the sample (along z).

(34) The value of R_{o} bears some degree of uncertainty. An issue of concern is the choice of the orientation factor ($3\kappa^2/2$) in eqs 1 and 3. This is a difficult problem. We have taken this factor as unity (pre-averaging). As indicated in the text, for most situations studied thus far this factor is within 10% of unity.[18] Because the orientation factor may be absorbed in R_{o}, by rewriting eq 1 as $w(r) = (R_{\mathrm{o}}'/r)^6/\tau_{\mathrm{D}}$, where $R_{\mathrm{o}}' = R_{\mathrm{o}}(3\kappa^2/2)^{1/6}$, one may conclude that an uncertainty in the orientation factor as high as 20% amounts to about 3% uncertainty in R_{o}, well within the variation range of R_{o} as determined experimentally ($R_{\mathrm{o}} = 2.3 \pm 0.1$ nm). The problem does not go away completely, however, because the formulation that leads to eqs 3 considers $3\kappa^2/2$ a constant in the pre-averaging sense.[16,25,26] As yet, a complete formulation of DET that includes generalized orientational effects has not been possible.

(35) For PS–PMMA we have $M_{\mathrm{n}}^{\mathrm{PS}}/M_{\mathrm{n}}^{\mathrm{PMMA}} = 40000/40000$ (gel permeation chromatography (GPC), NMR[10]), and in eq 5, $\chi = 0.041$.[36] For PI–PMMA we have $M_{\mathrm{n}}^{\mathrm{PI}}/M_{\mathrm{n}}^{\mathrm{PMMA}} = 10000/22000$ (GPC, NMR), and $\chi = 0.077$.[11] Knowledge of the characterization, however, does not affect the generation and/or analysis of our simulated data.

(36) Russell, T. P.; Helm, R. P.; Seeker, P. *Macromolecules* **1990**, *23*, 890.

(37) Anastasiadis, S. H.; Russell, T. P.; Satija, S. K.; Majkrzak, C. F. *J. Chem. Phys*. **1990**, *92*, 5677.

(38) (a) Russell, T. P.; Menelle, A.; Hamilton, W. A.; Smith, G. S.; Satija, S. K.; Majkrzak, C. F. *Macromolecules* **1991**, *24*, 5721. (b) Shull, K. R.; Mayes, A. M.; Russell, T. P. *Macromolecules* **1993**, *26*, 3929.

(39) Demas, J. N. *Excited-State Lifetime Measurements*; Academic Press: New York, 1983.

(40) O'Connor, D. V.; Phillips, D. *Time-Correlated Single Photon Counting*; Academic Press: London, 1984.

(41) Clearly, the description is somewhat subjective and depends on the choice of the peak intensity. In this work, the peak level is chosen as approximately 20 000 counts. In real experiments, depending on the sample, the time required to reach this level is about 1 h for labeled polymer films. Longer experiments, yielding higher peak counts, are not very practical, and the situation becomes more complicated because of lamp-drift problems. High-repetition laser excitation may overcome these problems.

(42) Hauser, M.; Klein, U. K. A.; Gösele, U. *Z. Phys. Chem*. **1976**, *101*, S255.

(43) Piessens, R.; de Doncker-Kapenga, E.; Überhuber, C. W.; Kahaner, D. K. *QUADPACK–A Subroutine Package for Automatic Integration*; Springer-Verlag: Berlin, 1983.

(44) Kahaner, D.; Moler, C.; Nash, S. *Numerical Methods and Software*; Prentice Hall: Englewood Cliffs, NJ, 1989.

(45) The Numerical Algorithms Group Limited. *NAG Fortran Library*, Mark 15; Oxford, UK, 1991.

(46) Garbow, B. S.; Hillstrom, K. E.; Moré, J. J. *Documentation for MINPACK Subroutine LMSTR. Double Precision Version*; Argonne National Laboratory, 1980.

(47) Grinvald, A.; Steinberg, I. Z. *Anal. Biochem*. **1974**, *59*, 583–598.

(48) Beechem, J. M.; Gratton, E.; Ameloot, M.; Knutson, J. R.; Brand, L. In *Topics in Fluorescence Spectroscopy*; Lakowicz, J. R., Ed.; Plenum Press: New York, 1991; Vol. 2, pp 241–305.